Journal of Materials Science: Materials in Electronics (2020) 31:15907–15918
https://doi.org/10.1007/s10854-020-04152-6

Effect of the electrolyte chemical nature on the formation and characteristics of TiO_2 nanotubes synthesized by anodic oxidation using a Ti cathode

A. C. Chávez-Mejía[1] · P. I. Zaragoza-Sánchez[1] · R. Magaña-López[1] · C. E. Barrera-Díaz[2] · B. E. Jiménez-Cisneros[1]

Received: 13 April 2020 / Accepted: 1 August 2020 / Published online: 13 August 2020

Abstract
The aim of this work is to show the effect of the electrolyte chemical nature on the formation of self-organized TiO_2 nanotubes (TNT) arrays synthesized via anodic oxidation, when using a Ti cathode. The synthesis was performed in situ in a potentiostatic cell provided with an anode and a cathode (both Ti substrates pretreated) under constant hydrodynamic conditions and different anodizing times, temperatures and electrical potentials. Ti electrodes were immersed in 300 mL of each of an inorganic and organic electrolyte. Then, a thermal treatment varying the temperature and the heating rate in each case was applied to convert the amorphous TiO_2 to crystalline TiO_2. TNT were characterized by field-emission scanning electron microscopy (FESEM), energy dispersive spectroscopy (EDS), X-ray diffraction (XRD) and atomic force microscopy (AFM). FESEM showed the formation of nanotubular structures perpendicular to Ti substrate with average inner diameters of 84 and 57 nm for TNT synthesized in the electrolytes with different nature tested (inorganic and organic), and labeled hereafter as TNT-I and TNT-O, respectively. EDS spectra from different zones of the substrate confirmed the presence of Ti (~ 34.2%) and O (~ 66%) on the surface of the TNT. The anatase (~ 86%) and rutile (~ 14%) crystalline phases were detected via XRD in both cases. AFM provided information about the topographic profile of TNT and the roughness of the substrates. Thus, the use of a semiconductor cathode allowed the successful synthesis of the TNT and the electrolyte chemical nature was found to influence its morphology, dimensions and formation mechanism.

1 Introduction

TiO_2 is a relatively abundant semiconductor material. Due to its excellent properties such as low toxicity, excellent stability to corrosion, and good chemical and biological stability, TiO_2 is used in the fabrication of solar and fuel cells, paints, cosmetics, inks printing, ceramics, textiles, pavements coverings, energy storage devices, hydrogen production, biomedical applications, and as a photocatalyst for water and air purification, metal oxidation, and inactivation of viruses and pathogenic microorganisms [1–9]. Nanostructured TiO_2 can be prepared in the form of a powder or thin films, produced using a variety of techniques such as thermal oxidation, spraying, chemical or physical deposition in the vapor phase, sol–gel, solvo-thermal processes, inverse micellar, and hydrothermal [7, 10–14]. However, these techniques have the disadvantage of needing expensive precursors and a long preparation time. Meanwhile, electrochemical techniques of Ti anodization and traditional techniques for oxide deposition on metals surfaces are very attractive since they

✉ P. I. Zaragoza-Sánchez
PZaragozaS@iingen.unam.mx

A. C. Chávez-Mejía
AChavezM@iingen.unam.mx

R. Magaña-López
RMaganaL@iingen.unam.mx

C. E. Barrera-Díaz
cebarrerad@uaemex.mx

B. E. Jiménez-Cisneros
BJimenezC@iingen.unam.mx

[1] Instituto de Ingeniería, Universidad Nacional Autónoma de México, Av. Universidad 3000, Coyoacán, C.P.04510 Mexico City, Mexico

[2] Centro Conjunto de Investigación en Química Sustentable UAEM – UNAM, Autopista Toluca – Atlacomulco 14.5 km, C.P. 50200 Toluca, State of Mexico, Mexico

do not require expensive reagents, they are highly reproducible, and have short production times. Such techniques can generate a thin film of anodic oxide that is compact or porous, amorphous or crystalline, strongly adhered to the metal surface, and thermodynamically stable in the pH range of 2–12 [7, 12, 15, 16]. Another advantage of electrochemical techniques is that they allow better synthesis control since the transformation of pure Ti into TiO_2 by potentiostatic anodization can be monitored using curves of current against time. As reported by various authors [12, 16–20], these curves can be used as a tool to predict the formation of TiO2 nanotubes (TNT). It is well known that by varying the experimental conditions in the electrochemical cell, such as the electrolyte concentration, voltage, and time of anodization, the anodic oxide will have differing physical characteristics, such as shape, dimension, color, density, homogeneity, and insulating properties [19, 21–25]. However, other anodization parameters such as the geometry, size, material, and cleaning of the electrodes; distance between the electrodes; type and speed of stirring; the pH, water content, temperature, and chemical nature of the electrolyte have been less studied, while regarding the reuse of electrolytes no report was found. Other characteristics such as a change in the volume of the electrolyte or the potential sweep speed do not affect the physical characteristics of the nanostructures [9, 12, 26–30].

The material of the electrodes is a determining factor of performance and cost of an anodization process. Metals (e.g., platinum, stainless steel, nickel) and carbon materials (e.g., graphite and activated carbon fiber) are the two most commonly used materials as cathodes for an electrochemical cell. Since the service life and stability are the most important characteristics for cathode material, platinum (Pt) is the most commonly cathode used in anodic oxidation processes because it is an excellent electrical conductor, does not oxidize easily, and has a longer service life and larger surface area [31]. Ti and Pt have similar properties such as a long service life and excellent electrical conductivity, which allows for good electron transfer. Both have excellent mechanical properties such as resistance, strength, and hardness, and excellent anti-corrosive properties. On the other hand, their chemical properties, particularly that they are not reactive (inert materials), make them good catalysts. However, one disadvantage of using Pt is that it is extremely expensive and very scarce when compared with Ti, which is cheaper and more abundant [32]. Therefore, in this work the use of a Ti cathode, taking advantage of its potential use as an anode, was more attractive.

Alternatively, the TiO_2 nanostructures that present characteristics such as biocompatibility, photocatalytic activity and superhydrophilicity have been found to offer great potential in biomedical applications, and photoelectrochemical and photocatalytic processes [8, 9, 21, 24, 29, 33–38]. In this regard, the advantage of TNT over other nanostructures such as nanoparticles, nanowires, nanobars, and nanofibers is the area provided by their internal and external surfaces.

In TNT synthesis by anodic oxidation, the electrolytes are prepared on fluorinated compounds such as NaF, HF, and NH_4F, and a supporting electrolyte such as ethylene glycol, glycerol, H_3PO_4, Na_2SO_4, $(NH_4)_2SO_4$, H_2SO_4, and $NaHCO_3$ dissolved in water [20]. As published previously [12, 17, 24, 39, 40], in the absence of the supporting electrolyte, the oxidation and hydrolysis of Ti is not uniformly catalyzed to produce an ordered nanoporous structure. In addition, in a fluorine-free electrolytic solution it is not possible to observe the formation of TNT; therefore, in this case only a compact layer of TiO_2 will be observed. Fluorine ions are responsible for TNT formation, since these ions tend to perforate the TiO_2 passive layer, resulting in a nanotubular morphology. For its part, the chemical nature of the electrolyte plays a very important role in determining the shape and dimensions of the TNT, and, in addition, other properties, such as its crystallinity, will depend on its efficiency [23, 41]. A thermal treatment of the anodized substrates at 300–350 °C generally allows the amorphous structure of the anodic oxide to transform into photoactive crystalline phases [4, 12, 19, 21, 24, 42–44]. Thus, using anodic oxidation, the pores of the TNT grow directly from the Ti substrate (TNT/Ti) generating good size, uniformity, order, electrical conductivity, and strong mechanical adhesion [9, 19, 44].

There are some studies about the synthesis of TNT previously published in the literature [11, 14, 45, 46]. Specifically, the synthesis of TNT using anodic oxidation is similar to the present work and has been published before by several authors [12, 16–19, 25, 42]. However, the aim of the present research was to further study the TNT formation process when synthesized in electrolytes of different chemical nature to compare their physical, chemical and structural characteristics, when a Ti electrode was used as a cathode compared to most of the works on TNT that use a Pt cathode. The bibliographic review did not find any reports in this regard. Therefore, it is expected the usage of a Ti cathode in the electrochemical system and the chemical nature of the electrolyte would affect the synthesis of the TNT. In addition, for this work, the electrolytes were reused several times, a question that has not been addressed elsewhere in the literature. The application of TNT as a photocatalyst for removing highly pathogenic viruses and emerging pollutants from drinking water [6, 8, 47] suggests that reducing costs for its production is an important goal in the environmental sciences. As such, in the current work, the exploration of material reuse to minimize chemical wastes and their impacts during the synthesis process may allow for a lower cost method that obtains the same, or even better, characteristics than traditional synthesizing methods.

2 Materials and methods

Pristine titanium foils (Ti, 99.7% purity, 0.127 mm thickness, Aldrich) were treated as follows: polished with different abrasive papers; sonicated in acetone (C_3H_6O, 99.99%, J. T. Baker), iso-propanol (C_3H_8O, analytical grade, J. T. Baker), and methanol (CH_4O, 99.97%, J. T. Baker); and exposed to a chemical attack with nitric acid (HNO_3, 65.1%, J. T. Baker) and hydrofluoric acid (HF, 48%, Aldrich). The foils were used as electrodes to synthesize TNT in inorganic (0.5 M H_3PO_4 85.7% and 0.14 M NaF 99%, J. T. Baker) and organic (0.5 wt% NH_4F 98%, 10 vol% H_2O and 90 vol% ethylene glycol 99.8%, Aldrich) electrolytes. The concentrations of these electrolytes were determined with reference to previous reports [18, 19, 42]. The electrolytes were prepared with high purity deionized water (resistivity = 18.2 MΩcm to 25 °C and TOC ≤ 5 µg L^{-1}) from the Milli-Q water system type Millipore advantage A10 Q-POD and reused in each anodization made.

2.1 Synthesis of TiO_2 nanotubes by anodic oxidation

The TNT synthesis was performed in situ via anodic oxidation of pure Ti substrates, in an inorganic and organic electrolyte, named as TNT-I and TNT-O in this study, respectively. The selection of electrolytes was based on an extensive literature review [12, 17, 21, 39, 40, 48, 49]. The steps followed during the process were done as recommended by [12, 16–19, 25, 42, 48]; although some of them were modified and detailed below.

2.1.1 Pre-treatment of titanium substrates

The Ti substrates were manually cut in rectangular strips and used as anode (1.5 cm × 2.0 cm) and cathode (3.0 cm × 3.7 cm). Then, they were polished with No. 400, 600, 1000 and 1200 silicon carbide abrasive papers using water as a lubricant to remove the passive oxide layer from the Ti surface caused by exposure to air. Next, the polished Ti substrates underwent a sonication process for 15 min using a BRANSON 2510 ultrasound equipment with 100 W ultrasonic waves to remove the residue of silicon carbide particles from the abrasive papers as well as any grease from the manual handling of the substrates. The sonification process used acetone, iso-propanol, methanol, and deionized water successively and according to their polarity. Afterward, the sonicated Ti substrates were chemically etched in an acidic mixture of $HF:HNO_3:H_2O$ in a volumetric ratio of 1:4:5 for 30 s to eliminate any superficial defects caused by the abrasive paper and to obtain a smooth and homogeneous surface. Finally, the Ti substrates were rinsed generously with deionized water, and then dried at room temperature (25 °C approximately). In this procedure, several Ti substrates were cleaned at once, but not all were anodized at the same time. To reduce the natural formation of a new passive layer of Ti oxide on unused Ti substrates, they were placed into a desiccator for a maximum of 3 h following cleaning and prior to anodization, as mentioned by [24, 50].

2.1.2 Anodic oxidation of titanium substrates

TNT-I and TNT-O synthesis were each performed in a potentiostatic cell provided with two electrodes. The pretreated Ti substrates previously described were used as electrodes. Then they were immersed in 300 mL of the electrolytes previously defined and their physicochemical characteristics were tested using a HACH 389 multiparameter equipment. The distance between the two electrodes was fixed at 3 ± 0.8 cm. The TNT-I synthesis was performed at 20 V with a scanning rate of 1 V s^{-1} during 45 min and the electrolyte temperature was maintained at 23 ± 0.7 °C. Alternatively, the TNT-O synthesis was performed at 30 V with a scanning rate of 1 V s^{-1} supplied during 60 min and with an electrolyte temperature of 30 ± 0.9 °C. A computer was used to send the tested voltage and anodization time data to a BK PRECISION 9184 power supply, and to monitor the electric current. The electrolytes were continuously stirred at 360 rpm to lead the synthesis throughout the entire experiment using a magnetic stirrer on a stirring and heating electric plate (CIMEREC Barnstead, Thermolyne). The temperature was controlled using a HANNA Instruments digital thermometer. An electrode connected to a HANNA Instruments 213 potentiometer was used to monitor the pH conditions. Values of time against electric current were recorded during the Ti anodization, and then plotted to predict the formation of TNT and to establish the mechanism. The experimental procedure for the synthesis of TNT is shown in Fig. 1.

2.1.3 Post-treatment of anodized titanium substrates.

After the anodic oxidation stage, a thermal treatment is fundamental for the transformation of the amorphous structure of TiO_2 into its crystalline phases [19, 44]. Then, the anodized substrates were washed generously with deionized water for 3 min to remove any occluded ions from the electrolytic solutions. The substrates anodized in the inorganic electrolyte were dried in a heating furnace RIOSSA at 100 °C for 13 h, and subsequently annealed using a LINDBERG 847 furnace increasing at a rate of 5°C min^{-1} and then held at 500 °C for three hours in ambient air composition. Meanwhile, the substrates anodized in the organic electrolyte were dried at room temperature (20–25 °C) for

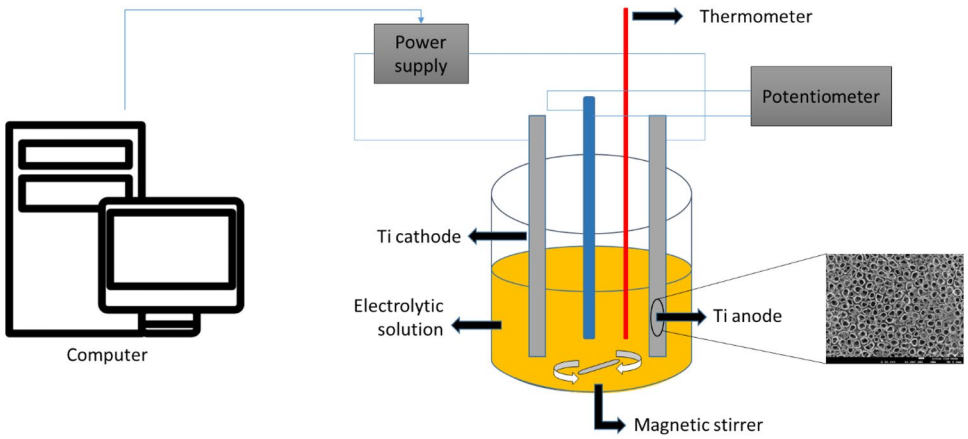

Fig. 1 Experimental procedure for the synthesis of TNT—anodic oxidation process

15 min, and then annealed using a heating rate at 3°C min^{-1} and held at 550 °C for 2 h in ambient air composition. In both cases, the anodized substrates were cooled slowly at room temperature (20–25 °C). Finally, all samples were then ready for their characterization.

2.2 Characterization of anodized titanium substrates

The nanostructure of the anodized substrates was characterized by field-emission scanning electron microscopy (FESEM, JEOL JSM 7600F, with accelerating voltage 1–30 kV and a maximum resolution 5 nm), and the surface morphology of the anodized substrates was characterized by atomic force microscopy (AFM, MFP-3D Origin). The elemental composition of the anodized substrates was analyzed by energy dispersive spectroscopy (EDS) attached with FESEM (OXFORD INCAX-ACT). The structural properties of the anodized substrates were determined by X-ray diffraction (XRD, Bruker D8 Advance powders diffractometer, LynxEye) with Cu Kα radiation (λ = 0.1540 Å) over an angular range between $20° \leq 2\theta \leq 80°$, with an increase in 2θ of 0.02° and 0.6 s per step [2, 51]. High-resolution transmission electron microscopy (HRTEM, JEOL JEM-ARM200F) analysis was used to observe the TNT-O bottom layer thickness.

3 Results and discussion

3.1 Synthesis of TiO_2 nanotubes

The TNT were obtained under different synthesis conditions as detailed in the methodology using electrolytes with the characteristics indicated in Table 1.

In Fig. 2, the substrates anodized in the inorganic electrolyte showed a litmus blue surface, while substrates anodized in the organic electrolyte showed a dark brown surface. As reported by [24, 38, 52], the colors are due to interference effects that are established in the metal-oxide-light interface. This indicates that both colored surfaces were covered by homogeneous TiO_2 films hundreds nanometers thick as mentioned by [12, 48, 53, 54].

Table 1 Physicochemical characteristics obtained for electrolytes

Parameter	Inorganic electrolyte	Organic electrolyte
pH	1.62	7.3
Conductivity (mS cm^{-1} at 20–25 °C)	23.1	1.13
Total dissolved solids (mg L^{-1})	15,140	562

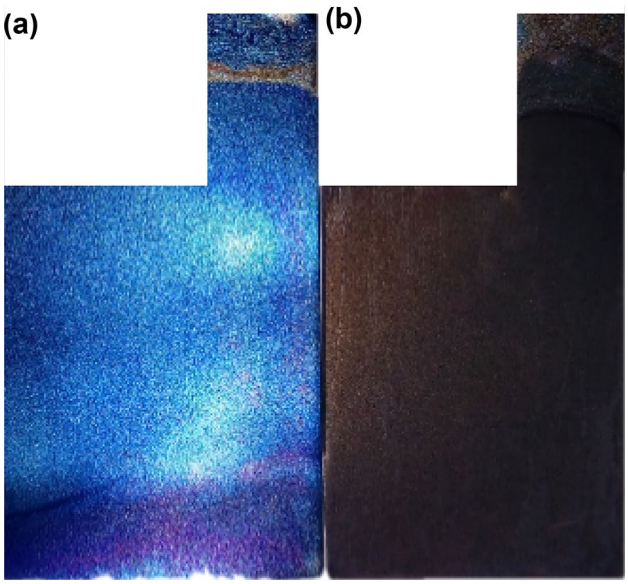

Fig. 2 Ti substrates anodized in **a** inorganic and **b** organic electrolytes

3.2 Characterization of the Ti substrates

3.2.1 Morphological characterization

The analysis was performed on different areas of the substrates using images generated with FESEM by the incidence of SEI electrons. Figure 3 corresponds to the surface of the pristine Ti substrate (no anodizated) purchased from Aldrich. The FESEM micrograph shows defects on the surface, confirming a necessary pre-treatment to remove defects such as curvatures or channels that could induce cracks and fracture points between the TNT [55].

Figure 4 depicts a series of micrographs from FESEM that correspond to the surface of the anodized substrates in both electrolytes (inorganic and organic) after thermal treatment. In Fig. 4, a porous layer on both faces of the substrate

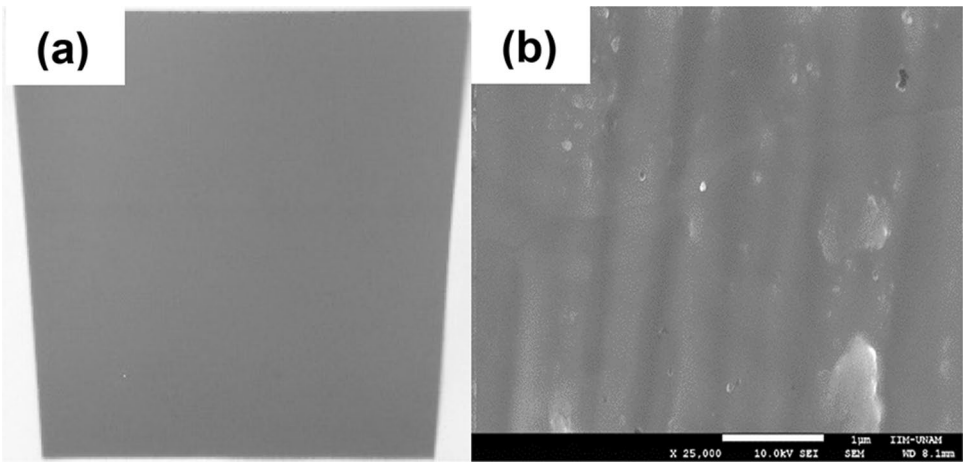

Fig. 3 **a** Surface of a pristine Ti substrate and its **b** FESEM micrography at 25,000X

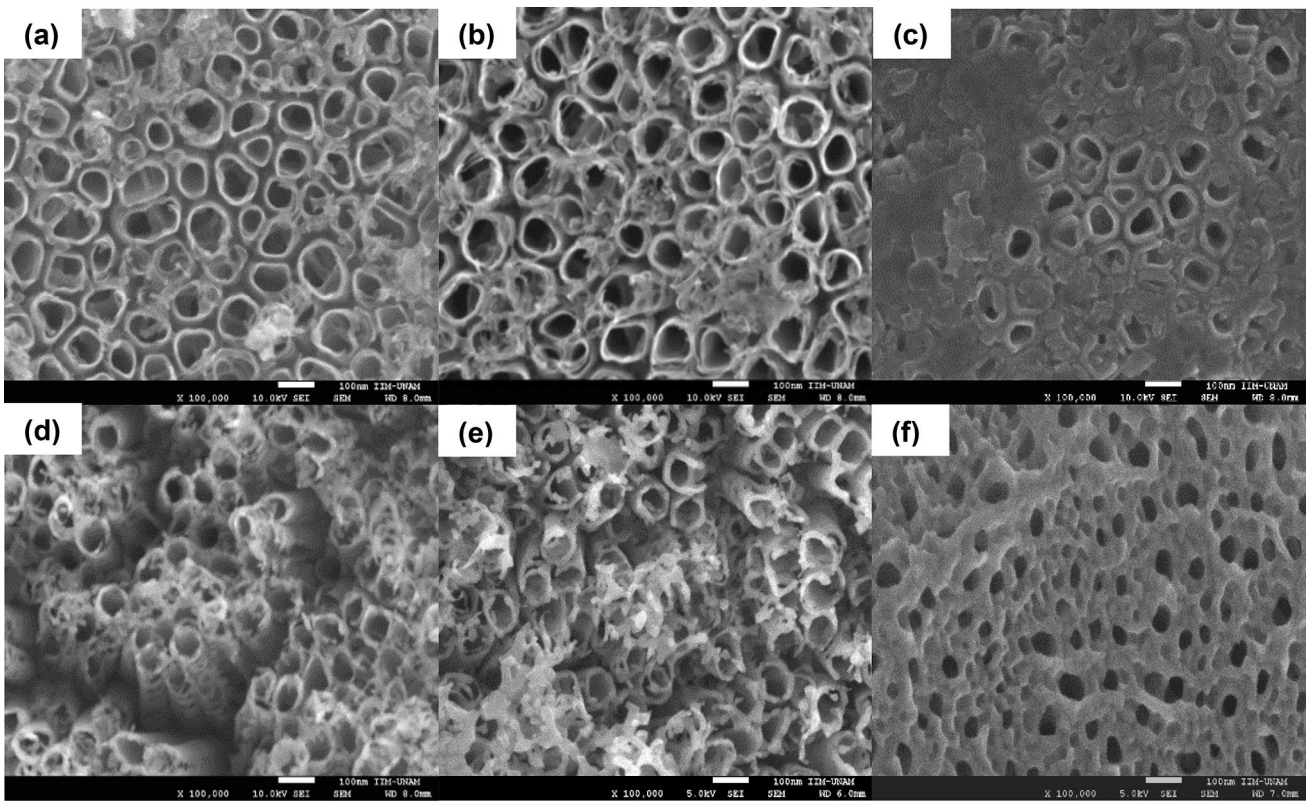

Fig. 4 FESEM micrographs of the anodized substrates at 100,000X in the inorganic (**a**–**c**) and organic (**d**–**f**) electrolyte showing: **a** and **d** top view-front, **b** and **e** top view-back, and **c** and **f** front view of the thickness of the Ti substrates

and on its spine, understood as thickness (0.127 mm), is observed. Therefore, the superficial area was doubled. Figure 4a shows the surface of the main face of the substrate anodized in the inorganic electrolyte (face of the substrate facing the cathode), while Fig. 4b shows the surface of its back face. On both sides of the substrate, a porous and uniform layer is observed over the entire surface and the depth (darker regions) in the pores can be appreciated. The observed depth in the pores indicates highly ordered arrays of long tubes have been formed. It is also observed that the diameter of the pores is very well defined. Figure 4c shows the formation of pores on the thickness of the substrates, although many of them appear to be blocked by a compact TiO_2 undissolved layer from the beginning of the anodization, called the passive layer [12, 55]. It is noted the diameter of the pores formed on the thickness of the substrates was less than that formed on the surface of their faces, and the absence of this layer of TiO_2 remained at 45 min. The aforementioned suggests a very fast speed of chemical dissolution of the TiO_2 (r_{cd}) formed, and an equilibrium between the rate of electrochemical formation of TiO_2 (r_{ef}) and the r_{cd} was reached quickly. Therefore, these observations indicated that the r_{cd} of TiO_2 over the thickness was slower than on the faces.

Figure 4d corresponds to the surface of the main face of anodized substrates in the organic electrolyte, while Fig. 4e shows the surface of its back face. In these figures, nanotubular structures form in different orientations but are favored in the z direction (as projective way) attaching at the top to form TNT-O clusters with abundant gaps among them, resulting in an apparently considerable length, as mentioned by [41]. On the substrates, a smaller tube diameter is observed on back face when compared to the main face, suggesting a slower TiO_2 dissolution. Figure 4f shows a nanoporous net formed on the thickness of the substrates, indicating that on the thickness the TNT-O are in the formation process.

In addition, the cross-sectional view of the substrates was analyzed to observe the TNT morphological profile (Fig. 5). Figure 5a corresponds to the cross section of the anodized substrates in the inorganic electrolyte. This figure shows the formation of a compact array of TNT-I, adjacent and parallel to each other, with a structural regularity that contrasts with their base, which indicates that there was uniformity in the length of the TNT-I. In addition, a conical shape is shown with an apparently rough outer wall that presents undulations, attributed to the high water content of the electrolyte as has been reported earlier by [9, 12]. In this figure, severe fractures along the TNT-I, seen as ruptures and tilt of the nanotubes wall are visible. This phenomenon is observed because the cutting technique used was not appropriate and can also be seen in the cross-sectional samples. Figure 5b corresponds to the side view of the anodized substrates in the organic electrolyte. In this figure, a compact array of long and thin tubes with smooth walls is observed. The TNT-O seems perpendicular to the Ti substrate. It is probable that the considerable longitudinal development of the TNT-O is due to the slow dissolution rate of the passive TiO_2 layer due to the relatively low electrolyte conductivity (1.13 mS cm^{-1}) and to its neutral pH. In the inset of Fig. 5b obtained by HRTEM the bottom layer thickness of the TNT-O is observable.

Table 2 compares the dimensions of the TNT obtained in this work with others reported in the literature. Nevertheless, no reports for the characterization of the thickness of the Ti substrates (spine) and the back face substrates were found.

The chemical nature of the electrolytes revealed changes in the morphology characterized by the shape and dimensions of the TNT [41]. Thus, the synthesis in the organic electrolyte produced TNT-O with smaller values for the face diameters (~ 57 nm), and thickness (~ 54 nm), thinner wall thicknesses (~ 14 nm), and bottom layer thickness (~ 48), and a larger value for the length (~ 2.3 µm) than the TNT-I with inner diameters on the faces, thickness, length, wall

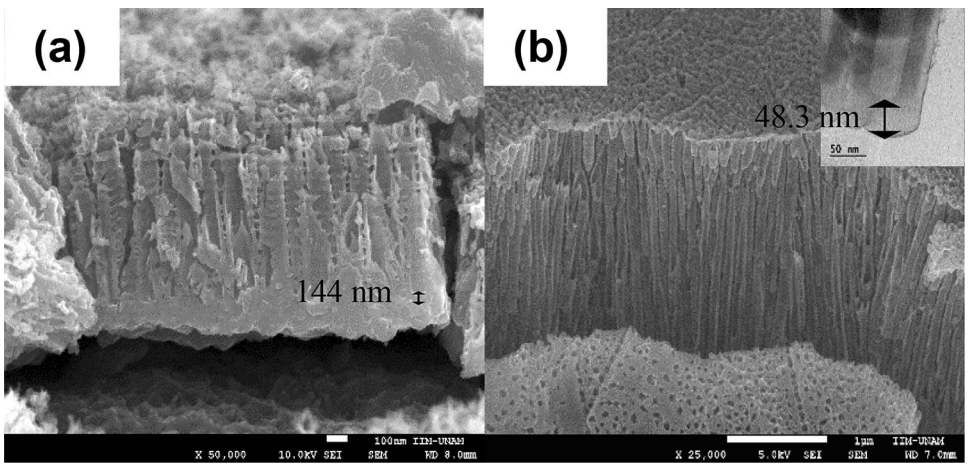

Fig. 5 FESEM micrographs at ×50,000 and ×25,000 from cross section of the anodized substrates in: **a** inorganic and **b** organic electrolyte. The inset in **b** from HRTEM depicts the bottom layer thickness of the TNT-O

Table 2 Comparison of the dimensions of the TNT synthesized in an inorganic and organic electrolyte

	Dimensions				Author
	Inner diameter (nm)	Length (μm)	Bottom layer thickness[a] (nm)	Wall thickness (nm)	
Synthesis in inorganic electrolyte	84.1 ± 22.7	0.77 ± 0.16	144 ± 44.0	18.3 ± 0.71	TNT-I obtained in this work
	120	0.6	–	15–20	[19]
	50–60	0.36	–	–	[26]
	90–130	0.5–0.65	–	–	[18, 39, 56]
Synthesis in organic electrolyte	57.0 ± 13.3	2.26 ± 0.35	48.3 ± 7.64	14.0 ± 0.00	TNT-O obtained in this work
	50	3.5	–	25–30	[19]
	50–90	1.5–4.5	–	–	[23, 42, 56]
	80–100	4.89	–	–	[42]
	50	0.75	–	15	[57]

[a]Bottom layer thickness refers to the remaining space between the internal and external nanotube walls at the bottom as in [12]

thickness, and bottom layer thickness of ~ 84 nm, ~ 74 nm, ~ 0.8 μm, ~ 18 nm, and ~ 144 nm, respectively. Therefore, it is assumed that the superficial area of the TNT-O was greater than the superficial area of the TNT-I. Additionally, there is clearly some minor inhomogeneity in the morphology of the TNT-O. On the other hand, according to [9, 12, 19], the properties of the chemical dissolution of TiO_2 to form TNT are influenced by the water content in the electrolyte. This aspect affects the TNT wall morphology. Thus, the TNT-I wall showed different characteristics when compared with the TNT-O wall. The TNT-I adopted a conical shape presenting undulations in the outer wall and giving an aspect of corrugated nanostructures, while the TNT-O adopted a cylindrical shape showing smooth walls with different thicknesses along the tube. This suggests that the mechanism of TNT formation in both electrolytes is significantly different and affects the resulting TNT morphology, dimensions, and, most likely, superficial area, which agrees with previous findings in the literature [12, 17, 19, 20]. It should be noted that in this work, the reuse of the electrolytes several times showed no alteration on the TNT morphological characteristics.

3.2.2 Elemental characterization

An EDS detector attached to the FESEM was used to determine the elemental composition from the surface of the samples. Thirty-three locations from anodized substrates in the inorganic and organic electrolytes and four from a sample of pristine Ti at 99.7% purity were analyzed. Representative spectra (Fig. 6a, b) from synthesis in both electrolytes confirmed the presence of Ti and O. A representative spectrum (Fig. 6c) from the sample of pristine Ti showed the presence of Ti (87.4 at. %), C (12.3 at. %), and Si (0.3 at. %). In the inset from Fig. 6c, the areas delimited by red circles correspond to the carbon deposited on the pristine Ti substrate.

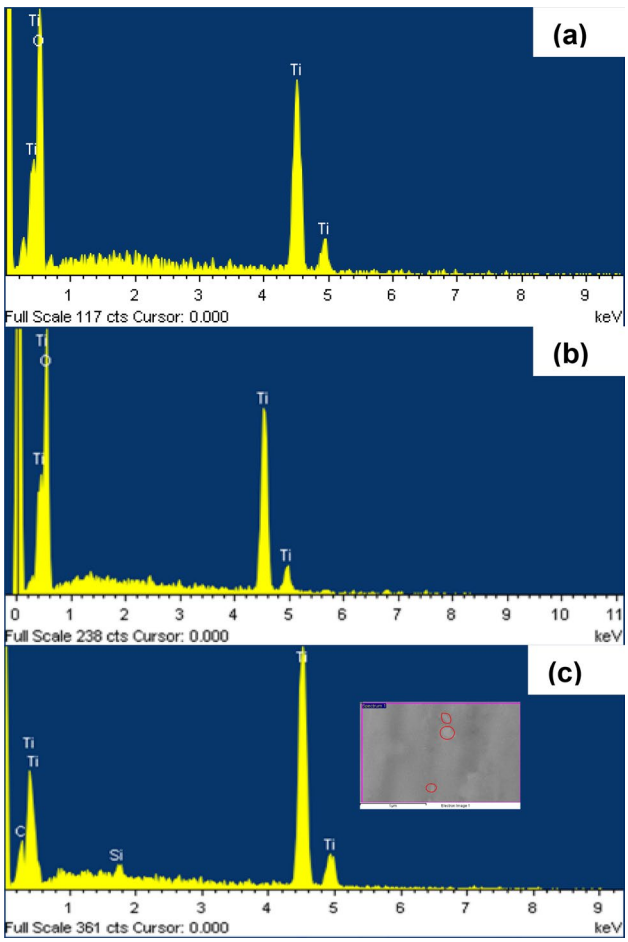

Fig. 6 EDS spectra from **a** TNT-I, **b** TNT-O and **c** pristine Ti substrate (99.7% purity). The inset in **c** depicts the surface morphology of the pristine Ti substrate with carbon impurities

This was attributed to traces of organic material (i.e., fatty material) left from the manipulation of the samples. Nevertheless, other impurities such as Si are typical of the substrate since it is not 100% pure.

Table 3 shows the average atomic percentages of each element referenced in Fig. 6. These findings showed that Ti and O contents on the surface of the TNT-I and TNT-O samples were similar and consistent with the atomic composition reported by [58]. However, [57] reported large differences in the composition. It is likely that the TiO_2 layer obtained by [57] is thinner than the one obtained in this work because the previous study was conducted in a nitrogen atmosphere while the current study was conducted in ambient air conditions.

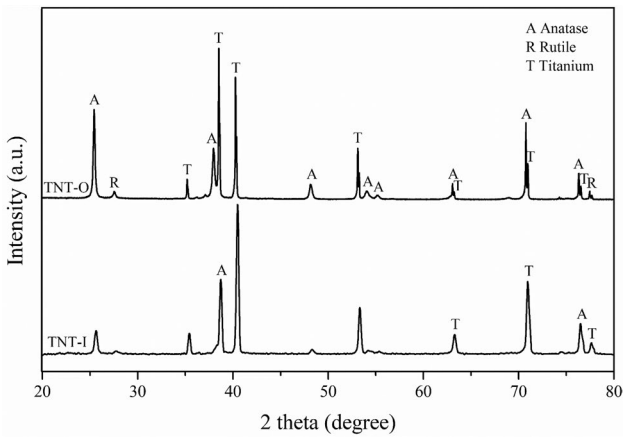

Fig. 7 X-ray diffraction patterns of the TNT-I and TNT-O

3.2.3 Structural characterization

The crystal structure of the TNT was determined using the diffractograms obtained from the XRD analysis (Fig. 7). The patterns exhibited by the TiO_2 in its anatase form constituted the dominant crystalline phase while only traces of rutile were detected. The diffractograms also showed some characteristic peaks for Ti attributed to the subjacent Ti substrate, as has been reported earlier [12, 19, 22, 42, 44, 57, 59, 60].

As shown in Fig. 7, the rutile/anatase relationship is different in both XRD patterns. The diffractogram from TNT-O showed a decrease in the Ti peak at 63.2°, 71°, and 76.5°, and subsequent appearance of anatase at 63.1°, 70.8°, and 76.3° 2θ. The conversion of Ti peaks to anatase peaks was attributed to the transformation of amorphous TiO_2 into its anatase crystalline phase. Other anatase peaks than those observed in the diffractogram from TNT-I as well as the appearance of rutile peaks at 27.5° and 77.5°, and traces of one at 36.2° and 56.7° 2θ were observed. This was likely due to the higher annealing temperature applied in the synthesis of the TNT-O (550 °C) with respect to that of the synthesis of TNT-I (500 °C). On the other hand, the intensities of these peaks were also affected, becoming more intense in TNT-O than TNT-I, meaning more crystallinity for TNT-O than TNT-I. However, the semiquantitative analysis in both samples indicated 86% of TiO_2 was found in the anatase phase and 14% in the rutile phase. The change in the intensity of the Ti peaks varies as the transformation of amorphous TiO_2 to crystalline TiO_2 takes place. The diameter of the TiO_2 crystals was calculated using the Debye–Scherrer equation and the results were compared with those reported by [61] as shown in Table 4. In this way, the greater size of the TNT-O crystals for the anatase phase was also attributed to the higher annealing temperature applied in the synthesis of the TNT-O. In comparison with this work, the absence of rutile crystals was reported by [61] as due to formation of only the anatase phase when conducting the experimental work at a lower temperature [43, 44]. According to the studies carried out by [43], a mixture of rutile (28.1%) and anatase (71.9%) is formed at 600 °C, while 100% of the anatase phase is exhibited at 300 °C, 400 °C, and 500 °C. In [61] the authors used a lower temperature (at 450 °C) than those used in this work (at 500 °C and 550 °C). Therefore, the formation of ~ 14% rutile and ~ 86% anatase is possible between 500 and 600 °C [44]. Thus, the formation of the two crystal phases was attributed to the annealing temperature and the percentages were obtained by a semiquantitative XRD analysis.

3.2.4 Topographic and textural characterization

Figure 8a shows the three-dimensional structure visible in the topographic image in the 10 × 10 µm range of the TNT-I with a root mean square (RMS) of 72.18 nm and a maximum background-peak distance close to 0.68 µm. Figure 8b shows the surface topography of TNT-O with a RMS of 145.27 nm and the maximum peak height was 0.85 µm. The roughness is noticeably different between the two samples, thus, while

Table 3 Average composition (at.%) of the surface of the TNT determined by an EDS detector attached to the FESEM

Element	TNT-I	TNT-O	[57]	[58]
O	63.32	68.37	34.76	66.63
Ti	36.68	31.63	65.24	33.36

Table 4 TiO_2 crystallite size

Crystal structure of the TNT	Present work		[61]
	TNT-I	TNT-O	
Anatase	12 nm	28 nm	25 nm
Rutile	24 nm	54 nm	–

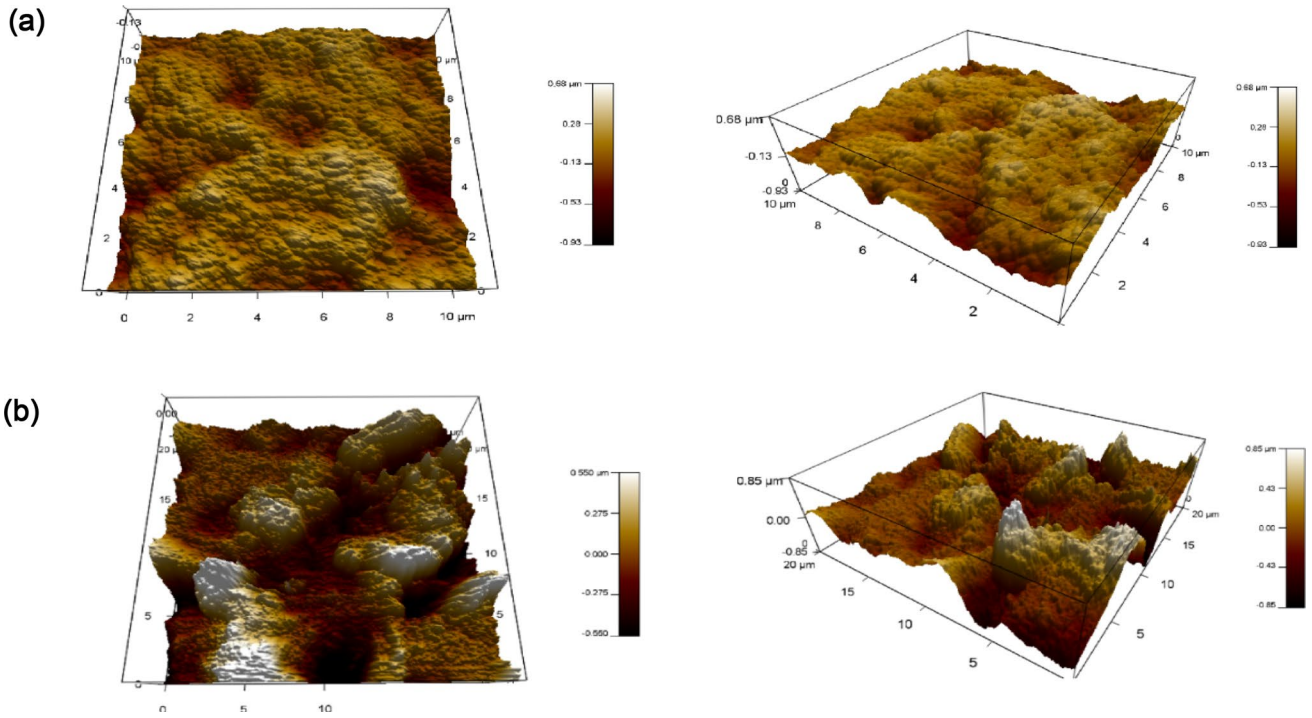

Fig. 8 Topographic profile of the **a** TNT-I and **b** TNT-O

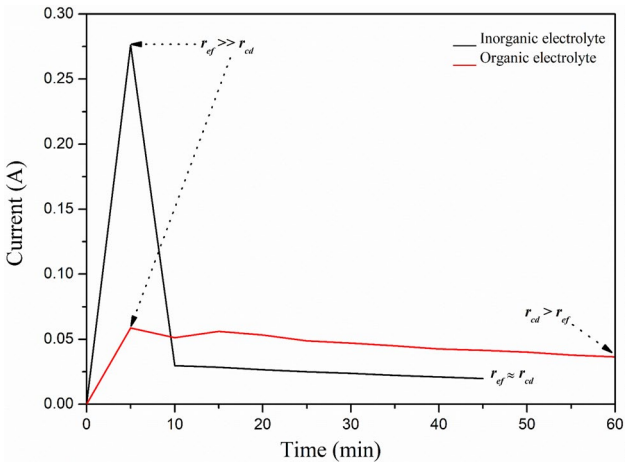

Fig. 9 Time profiles *vs* current during anodization of Ti in the inorganic and organic electrolytes

TNT-I shown a better homogeneity in distribution and peak height, large irregularities were obtained on the surface of the TNT-O, probably helping to increase the superficial area [55].

3.3 Relationship between the current curves and the TNT formation

During the Ti anodization, the behavior of the electric current as a function of time was recorded and the values were plotted as shown in Fig. 9. This figure compares the current profiles achieved in the two electrolytes.

In the initial stages, the electric current recorded in the synthesis of the TNT-I reached maximum values around 0.28 A at 5 min of the process, i.e., values almost five times higher than those reached in the synthesis of the TNT-O due to its acidic pH, high conductivity, and high water content as was previously reported by [12]. Subsequently, the current decreased abruptly to approximately 0.03 A, indicating the formation of a thin and compact layer of TiO_2 (passive layer). Thus, after 5 min, the current values observed in the inorganic electrolyte were lower than those observed in the organic electrolyte. This fact was attributed to the quick saturation of the electric current because of the rapid formation of the passive layer of TiO_2. Finally, the decreasing trend continued during the remaining anodization period at an almost imperceptible speed, and at approximately 15 min it began to saturate to a constant value indicating that repassivation was about to occur. Therefore, in the inorganic electrolyte, the drastic decrease and subsequent saturation of the current indicates the fast speed of formation of the passive layer of TiO_2 and of the TNT-I, respectively [12, 16–20].

On the other hand, in TNT-O synthesis, at 5 min the electric current reached a maximum value of the order of 0.06 A, and then began to decrease moderately. This decrease is related to the competition between the development of the compact layer of TiO_2 and the process of pore formation. Then, at 10 min, a point of inflection was observed

indicating the formation of the compact layer of TiO_2 as the dominant process for this period. Subsequently, the current began to increase until the curve adopted a convex shape (with a second maximum at 0.056 A) marking the beginning of the formation of pores and subsequent growth of the TNT-O. Immediately after this, the curve was preceded by a slow drop of current because of the longitudinal growth of the TNT-O. This continued until the end of the process showing the development of the repassivation. In this way, the gradual decrease of the current revealed a slow dissolution speed of the TiO_2 layer and then, a slow formation and development of the TNT-O. This behavior of the current is similar to that previously reported in the literature for electrolytes containing fluoride in aqueous solution [12, 16–20].

Therefore, when comparing the current curves from Fig. 9, it can be concluded that the rate of formation of the TNT-I was significantly faster than that of the TNT-O, i.e., in the inorganic electrolyte the equilibrium point between the r_{ef} and the r_{cd} was reached quickly. In addition, the behavior of the curves from Fig. 9 was consistent with that reported by several authors [12, 16–20, 54, 57, 62], who observed in general that the current decays logarithmically until a minimum value takes place during the formation of the passive layer of TiO_2, which later stabilizes. In this work and according observations by those authors, when the current decreased and then stabilized, the formation of a tubular layer of TiO_2 on the surface of the substrate had reached a thickness limit. This behavior is adapted to the mechanism of formation of the TNT established for aqueous systems with additions of fluorine, consisting of the stages that are schematized in the Fig. 10. It should be noted that, in the acid electrolyte of pH 1.62 the high speed of TNT-I formation compared to the speed of formation of TNT-O in the organic electrolyte of pH 7.3 can be explained by the increased mobility of fluoridated species through diffusion of the F^- ions and, the effusion of the $[TiF_6]^{-2}$ ions inside and outside the nanotubular reaction channel, respectively [18, 20].

The mechanisms of formation of synthesized TNT in both electrolytes (inorganic and organic) is in agreement of those reported in literature [12, 17, 18, 20, 39, 54], since similar current profiles denote an abrupt decrease in the initial stage. The aforementioned is due to the formation of a compact layer of TiO_2 that is gradually stabilized until it reaches a stable state signifying the dissolution of compacted TiO_2 by the fluorine ions. Figure 10 presents the formation and growth stages of the TNT from the anodization sequentially at different anodization times from 5 min until 60 min. On the left side of Fig. 10, the sequence of FESEM images corresponding to TNT-I indicates the random formation of a microporous layer at the first 5 min of anodization. Next, at 10 min the micropores are present on the entire surface of TiO_2. Subsequently, from 20 min these pores grow until acquiring a pronounced depth at 30 min. Later, at 45 min the pores are separated to form individual self-ordered tubular nanostructures. Finally, the dilatation of the pores and the reduction of their thickness is evident at 60 min. On the right side of Fig. 10, the mechanism of formation of the TNT-O is presented, starting at the first 5 min when the passive layer was formed. Then, the passive layer is followed by a stage of thickening at 10 min and subsequent microfissuring at 20 min of anodization. Subsequently, at 30 min the pores grow disorderly in both diameter and depth. At 45 min the porous structure acquires a well-defined nanotubular structure formed by common walls between adjacent TNT. Finally, by 60 min the nanotubular structure continues its longitudinal development, separation, pore dilatation, and thinning of the walls of the TNT-O. Then, it is concluded that, until minute 30, the kinetics of formation of TNT-O is slower than that of TNT-I. Therefore, the chemical nature of the electrolyte is a factor that affects the speed and the mechanism of formation of the TNT. Thus, the TNT formation mechanism can be described in general terms as: (1) formation of a thin and compact layer of TiO_2 (passive layer) during first few minutes of anodization, (2) thickening of the passive layer and subsequent pore nucleation, (3) formation and growth of a porous layer, (4) formation of nanotubular structures, and (5) dimensional development of the nanotubular structures [55].

The pore formation is a complex process. Chemically during the process of anodic oxidation in an aqueous electrolyte the Ti is oxidized to form TiO_2 according to the reactions (oxide-reduction) mentioned in Eqs. 1 and 2. A complexing ligand (F^-) leads to localized and substantial dissolution of the pores, generating a pH gradient between the bottom and the mouth of the pores until repassivation occurs [12, 15, 16]. Thus, the formation of TNT is given by the reaction indicated in Eq. 3 [18, 20, 25, 63].

$$2H_2O \rightarrow O_2 + 4e^- + 4H^+ \quad (1)$$

$$Ti + O_2 \rightarrow TiO_2 \quad (2)$$

$$TiO_2 + 6F^- + 4H^+ \rightarrow \left[TiF_6\right]^{-2} + 2H_2O \quad (3)$$

According to these reactions, amorphous TiO_2 formation generally occurs by the migration of Ti^{+4} ions from the anode toward the electrolyte and by the migration of O_2 from electrolyte to the anode. Subsequently, the nanotubular form is produced by the migration of fluorine ions (with faster penetration than observed for O_2) and ions $[TiF_6]^{-2}$ toward the interior and exterior of the pores of TiO_2, respectively [20, 54]. Thus, the formation of TNT is a direct consequence of the competition between the r_{ef} referred to oxidation speed of the pure Ti and the r_{cd} of the newly formed TiO_2

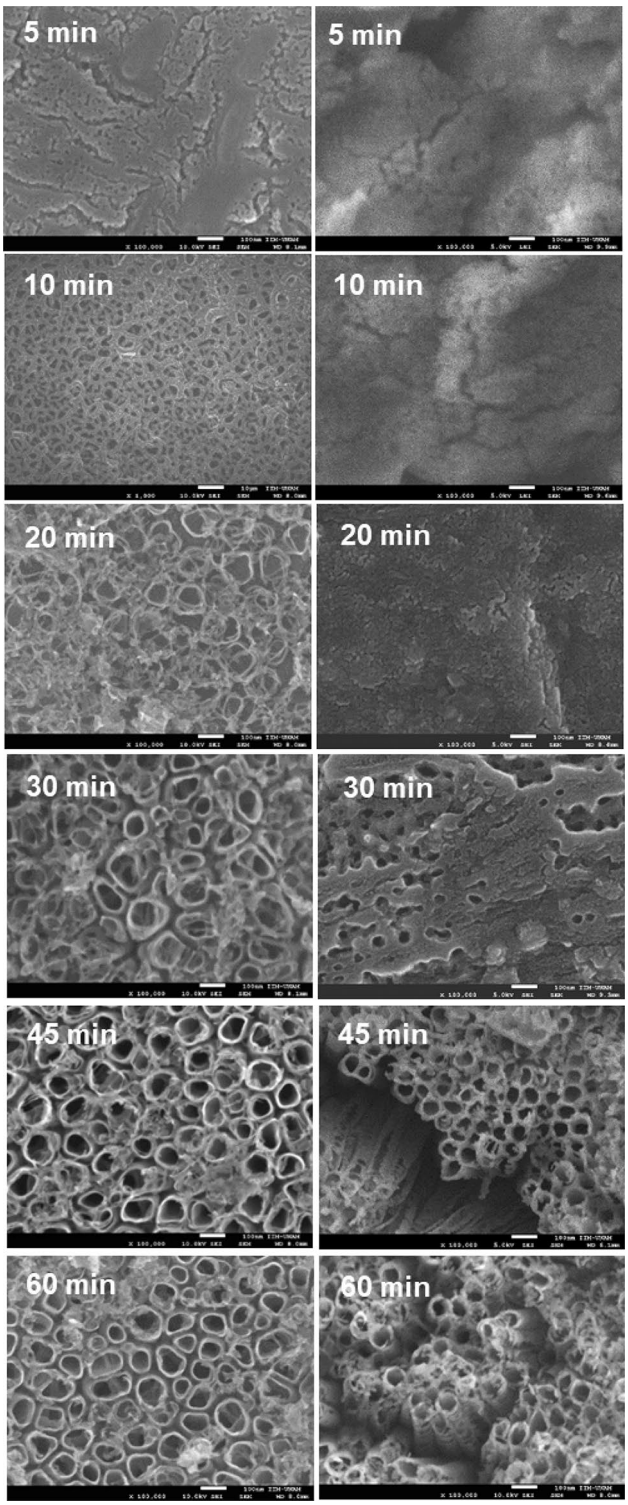

Fig. 10 Mechanism of formation of TNT-I (left column) and TNT-O (right column) at different times

due to the F^- ions of the electrolyte. The relation r_{ef}/r_{cd} is the one that will determine if the formation of the TNT begins.

4 Conclusions

Using a Ti foil as a cathode, successful synthesis of TNT was achieved in inorganic and organic electrolytes. Their chemical nature influence on the morphology, dimensions, mechanism, and speed of formation of the TNT without affecting their chemical composition. Crystalline TNT-I and TNT-O with potential photocatalytic activity were obtained after an annealing process at 500 °C and 550 °C, respectively. TNT of smaller diameter, greater length, and probably greater superficial area were obtained using the organic electrolyte, while the opposite was found when the inorganic electrolyte was used. Alternatively, a greater uniformity in the morphology, roughness, and ordering of the TNT-I was observed than that in the TNT-O. Likewise, formation of TNT-I was much faster than that of TNT-O. Finally, the electrolyte reuse does not affect the nanotubes formation. Moreover, for further researching about electrolyte reuse it would be helpful to explore the structural and physicochemical characteristics, formation mechanism, and how is this influenced.

Acknowledgements The authors would like to thank the Materials Research Institute of UNAM (IIM-UNAM), especially the University Electron Microscopy Laboratory (LUME) for their support in conducting FESEM and EDS analysis. We are also grateful to the Joint Center for Research in Sustainable Chemistry UAEM-UNAM (CCIQS), especially the X-ray Diffraction and Microscopy Laboratories for performing the XRD and AFM analysis, respectively. We also thank the Engineering Institute-UNAM especially to Environmental Engineering Laboratory (LIA) for providing its facilities. RML would like to thank DGAPA andCTIC for the grant received for postdoctoral studies at II-UNAM.

Compliance with ethical standards

Conflict of interest The authors declare that they have no conflict of interest.

References

1. D. Mardare, G.I. Rusu, Mater. Sci. Eng. **515**, 68 (2000)
2. M. Hamadanian, A. Reisi-Vanani, A. Majedi, Mater. Chem. Phys. **116**, 376 (2009)
3. Y. Ohama, D. Van Gemert, *Application of Titanium Dioxide Photocatalysis to Construction Materials*, 5th edn. (Springer, Dordrecht, 2011), pp. 1–56

4. J. Augustynski, B.D. Alexander, R. Solarska, Metal Oxide Photoanodes for Water Splitting Photocatalysis, ed. By C.A. Bignozzi (Springer, Heidelberg, 2011), p. 10
5. Y.I. Gaya, *Heterogeneous Photocatalysis Using Inorganic Semiconductor Solids* (Springer, Dordrecht, 2014), pp. 1–205
6. M.N. Chong, B. Jin, C.W.K. Chow, C. Saint, Water Res. **44**, 2997 (2010)
7. M. Abdullah, S.K. Kamarudin, Renew. Sust. Energ. Rev. **76**, 212 (2017)
8. M. Abidi, A. Hajjaji, A. Bouzaza, K. Trablesi, H. Makhlouf, S. Rtimi, A.A. Assadi, B. Bessais, J. Photochem. Photobiol. A **400**, 112722 (2020)
9. V. Sivaprakash, R. Narayanan, Mater. Today, (2020)
10. E.R.L. Tiburtius, P. Peralta-Zamora, E.S. Leal, Quim. Nova **27**, 441 (2004)
11. X. Ji-Chuan, L. Mei, G. Xin-Yong, L. Hu-Lin, J Mol Catal A Chem **226**, 123 (2005)
12. J. Macak, H. Hildebrand, U. Marten, P. Schmuki, J. Electroanal. Chem. **621**, 254 (2008)
13. S. Ahmed, M.G. Rasul, R. Brown, M.A. Hashib, J. Environ. Manag. **92**, 311 (2011)
14. Y.L. Pang, A.Z. Abdullah, Appl. Catal. B **129**, 473 (2013)
15. M. Paulose, H.E. Prakasam, O.K. Varghese, L. Peng, K.C. Popat, G.K. Mor, T.A. Desai, C.A. Grimes, J. Phys. Chem. C. **111**, 14992 (2007)
16. Z.B. Xie, D.J. Blackwood, Electrochim. Acta **56**, 905 (2010)
17. K.S. Raja, M. Misra, K. Paramguru, Electrochim. Acta **51**, 154 (2005)
18. S.K. Mohapatra, M. Misra, V.K. Mahajan, K.S. Raja, J. Catal. **246**, 362 (2007)
19. M. Asma, J. Lorna, B. Mohammad, R. Wan, Ceram. Int. **39**, 3731 (2013)
20. C. Shiyi, C. Qun, G. Mingqi, Y. Shuo, J. Rong, Z. Xufei, Surf. Coat. Technol. **321**, 257 (2017)
21. M.V. Diamanti, M.P. Pedeferri, Corros. Sci. **49**, 939 (2007)
22. N. Masahashi, S. Semboshi, N. Ohtsu, M. Oku, Thin Solid Films **516**, 7488 (2008)
23. H.-Y. Chang, W.-J. Tzeng, S.-Y. Cheng, Solid State Ion. **180**, 817 (2009)
24. M.V. Diamanti, F.C. Spreafico, M.P. Pedeferri, Phys. Procedia **40**, 30 (2013)
25. S. Poddar, A. Bit, S.K. Sinha, Mater. Chem. Phys. **254**, 123457 (2020)
26. V. Jaeger, W. Wilson, V. Subramanian, Appl. Catal. B **110**, 6 (2011)
27. G. Ali, M. Maqbool, Mater. Chem. Phys. **233**, 21 (2019)
28. D.E. Kim, D. Pak, Chemosphere **228**, 611 (2019)
29. L. Huang, D. Li, J. Liu, L. Yang, C. Dai, N. Ren, Y. Feng, J. Hazard. Mater. **393**, 122329 (2020)
30. A.V. Lashkov, F.S. Fedorov, MYu Vasilkov, A.V. Kochetkov, I.V. Belyaev, I.A. Plugin, A.S. Varezhnikov, A.N. Filipenko, S.A. Romanov, A.G. Nasibulin, G. Korotcenkov, V.V. Sysoev, Sens. Actuators B Chem. **306**, 127615 (2020)
31. C. Zhang, Y. Jiang, Y. Li, Z. Hu, L. Zhou, M. Zhou, Chem. Eng. J. **228**, 455 (2013)
32. J. Lario-Femenía, A. Amigó-Mata, A. Vicente-Escuder, F. Segovia-López, V. Amigó-Borrás, Rev. Metal. **52**, 4 (2016)
33. A. Mills, S. Le Hunte, J. Photochem. Photobiol. A **108**, 1 (1997)
34. N. Serpone, J. Photochem. Photobiol. A **104**, 1 (1997)
35. T. Ohtsuka, T. Otsuki, Corros. Sci. **40**, 951 (1998)
36. A. Fujishima, T.N. Rao, D.A. Tryk, J. Photochem. Photobiol. C **1**, 1 (2000)
37. O. Carp, C. Huisman, A. Reller, Prog. Solid State Chem. **32**, 33 (2004)
38. M.F. Brunella, M.V. Diamanti, M.P. Pedeferri, F. Di Fonzo, C.S. Casari, A. Li Bassi, Thin Solid Films **515**, 6309 (2007)
39. J.M. Macak, K. Sirotna, P. Schmuki, Electrochim. Acta **50**, 3679 (2005)
40. A. Ghicov, H. Tsuchiya, J.M. Macak, P. Schmuki, Electrochem. Commun. **7**, 505 (2005)
41. D. Niu, A. Han, H. Cheng, S. Ma, M. Tian, L. Liu, Chem. Phys. Lett. **735**, 136776 (2019)
42. L. Hailei, C. Lixin, L. Wei, S. Ge, D. Bohua, Ceram. Int. **38**, 5791 (2012)
43. J. Yu, B. Wang, Appl. Catal. B **94**, 295 (2010)
44. M. Motola, L. Hromadko, J. Prikryl, H. Sopha, M. Krbal, J.M. Macak, Electrochim. Acta **352**, 136479 (2020)
45. W. Shaohua, Z. Shaoqi, J. Hazar. Mater. **185**, 77 (2011)
46. D.J. Park, T. Sekino, S. Tsukuda, S.-I. Tanaka, Res. Chem. Intermed. **39**, 1581 (2013)
47. A. Chávez-Mejía, A. Chávez-Velasco, P. Zaragoza-Sánchez, B. Jiménez-Cisneros, Membranes: Materials, simulations, and Applications, ed. By A. Maciel-Cerda (Springer, Switzerland, 2017), p. 105
48. M. Bestetti, S. Franz, M. Cuzzolin, P. Arosio, P.L. Cavallotti, Thin Solid Films **515**, 5253 (2007)
49. N. Ohtsu, S. Komiya, K. Kodama, Thin Solid Films **534**, 70 (2013)
50. M.V. Diamanti, M. Ormellese, M.P. Pedeferri, Corros. Sci. **52**, 1824 (2010)
51. D. Shuxi, W. Yanqiang, S. Toshio, D. Zuliang, S. Hideki, A. Masahiko, Nanoscale Res. Lett. **5**, 1829 (2010)
52. Q. Wang, X. Yang, X. Wang, M. Huang, J. Hou, Electrochim. Acta **62**, 158 (2012)
53. L. Chin-Jung, Y. Wen-Yueh, L. Yen-Tien, C. Shu-Hua, *Chem. Commun.* 6031 (2008)
54. S. Berger, J. Kunze, P. Schmuki, D. LeClere, A.T. Valota, P. Skeldon, G.E. Thompson, Electrochim. Acta **54**, 5942 (2009)
55. V. Asgari, M. Noormohammadi, A. Ramazani, M.A. Kashi, Corros. Sci. **136**, 38 (2018)
56. R. Beranek, H. Tsuchiya, T. Sugishima, J.M. Macak, L. Taveira, S. Fujimoto, H. Kisch, P. Schmuki, Appl. Phys. Lett. **87**, 243114 (2005)
57. Y.S. Sohn, Y.R. Smith, M. Misra, V. Subramanian, Appl. Catal. B **84**, 372 (2008)
58. T.A. Saleh, V.K. Gupta, J. Colloid Interface Sci. **371**, 101 (2012)
59. K. Pan, M. Tian, Z.-H. Jiang, B. Kjartanson, A. Chen, Electrochim. Acta **60**, 147 (2012)
60. P. Acevedo-Peña, J.E. Carrera-Crespo, F. González, I. González, Electrochim. Acta **140**, 564 (2014)
61. X.-M. Song, J.-M. Wu, M. Yan, Thin Solid Films **517**, 4341 (2009)
62. H. Sopha, Y. Norikawa, M. Motola, L. Hromadko, J. Rodriguez-Pereira, J. Cerny, T. Nohira, K. Yasuda, J.M. Macak, Electrochem. Commun., (2020)
63. H.H. Park, I.S. Park, K.S. Kim, W.Y. Jeon, B.K. Park, H.S. Kim, T.S. Bae, M.H. Lee, Electrochim. Acta **55**, 6109 (2010)